29th Congress of the International Council of the Aeronautical Sciences
St. Petersburg, Russia; September 7-12, 2014

SIMULATION OF AN ALL-ELECTRIC FLIGHT CONTROL SYSTEM FOR THE EVALUATION OF POWER CONSUMPTION

Schettini F. *, Denti E. *, Di Rito G. * and Galatolo R. *
***Università di Pisa, Dipartimento di Ingegneria Civile e Industriale - Sez. Aerospaziale**

Keywords: *all-electric, electro-mechanical actuation, hinge moment*

Abstract

The complete electrification of aircraft power systems entails the implementation of smart logics for sharing the available energy among the loads, and the design of these logics requires the characterisation of the power absorption of each on-board system as a function of mission phase and aircraft operating point, also taking into account the level of criticality of the function implemented by the system itself.

The paper describes the models of the electro-mechanical systems used for the flight control actuation of a regional aircraft, with the basic objective of evaluating the power requests that have to be fulfilled both continuously and completely for this safety-critical equipment.

The Flight Control System (FCS) model is composed of both primary and secondary flight controls. The control surfaces are driven by Electro-Mechanical Actuators (EMAs) and all the EMA models refer to actuators with a 3-phase synchronous brushless motor and mechanical transmission.

Simulation tests have been performed to assess the maximum power flows characterizing the system, with reference to severe operative conditions.

1 Introduction

The design of modern airborne systems and equipments constantly tends towards both technology innovation and integration of functions. This trend has been recently emphasized by research programs oriented to the conversion of aircraft systems to the "all-electric" solution [1][2][3][4], which, together with well-known advantages in terms of eco-sustainability and costs reduction, point out important issues on power management for systems [5][6][7]. Actually, in the conventional aircraft technological frame, different types of power are derived from the engine for supplying the on-board systems: pneumatic, hydraulic, mechanical and electrical. The All-Electric Aircraft (AEA) concept is instead based on the replacement of hydraulic and pneumatic power with the electrical one, so that the suggestive acronym PbW (Power by Wire) has been coined for referring to a solution that satisfies all power requests by cables. As for any technological innovation, new issues related to performances and reliability are expected, as well as systems interactions concerns in terms of electrical power flows. The challenging all-electric objective can be thus achieved by appropriately monitoring and managing the power requests (e.g. by temporarily reducing the power supplied to some systems during those flight phases in which the total request of electrical power could overcome the maximum available). Energy Management System (EMS) logics need to be used, starting from the characterisation of the power absorption of each on-board system as a function of mission phase and aircraft operating point. In this context, a strong effort is required for system engineers to develop models that are capable of predicting the aircraft systems power flows. Modelling and simulation activities play a key role in this design loop: firstly, because the power management can be simulated in operating conditions that are difficult to be tested in flight or via on-ground

rigs, pointing out criticalities; secondly, because the electro-mechanical actuation is a novel technology for flight controls and the influence on performances of electrical power quality, actuator thermal behaviour and power electronics efficiency needs to be investigated and predicted.

2 Model description

2.1 Flight Control System data

The model is developed with reference to a FCS composed of the following control surfaces (Fig. 1):

- Primary flight controls
  - Ailerons and Steering Spoilers for roll control;
  - Elevators for pitch control;
  - Rudder for yaw control.
- Secondary flight controls
  - Inboard and outboard Flaps

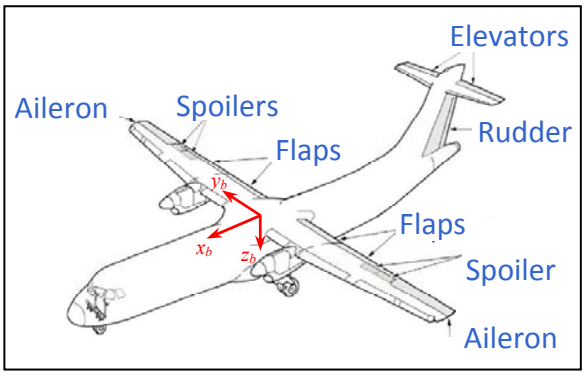

Fig. 1. Flight control system layout

2.2 Basic simulation scheme

The FCS models have been developed by using for each control surface the basic Matlab-Simulink scheme depicted in Fig. 2.

Essentially, the basic scheme is composed of two main models: an EMA model and a dynamics and kinematics model of control surface. It is worth noting the strong interaction existing between these two models. EMA model evaluates the actuator rod dynamics, whose acceleration, velocity and position are needed to the dynamics and kinematics model to provide the force acting on EMA itself. This interaction determines an algebraic loop in the Simulink scheme that has been solved by applying an integration step delay (memory block) on the force signal.

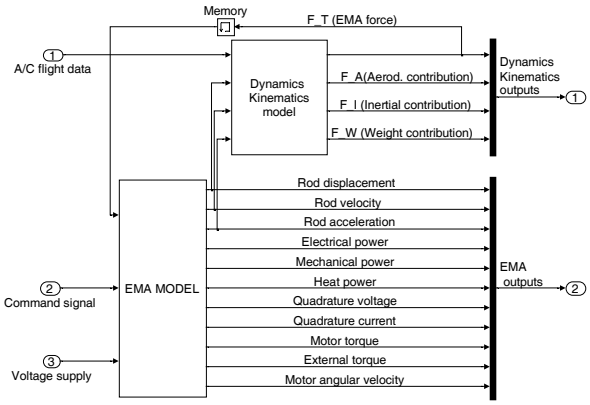

Fig. 2. Matlab-Simulink Basic model

2.3 EMA model

The functional model of the EMA system has been developed under the following assumptions:

- the 3-phase brushless motor dynamics is described in the *dq0* frame (no Park transforms are used) neglecting the homopolar axis
- the power electronics is ideal (no voltage drop on a closed switch, no current through an opened switch, perfect voltage tracking)
- the mechanical transmission is perfectly rigid

The electric equations along the direct and quadrant axes of the motor are thus given by Eqs. (1)-(2),

$$V_d = R\,i_d + L_d \frac{di_d}{dt} - L_q p_m\, i_q\, \omega_m \qquad (1)$$

$$V_q = R\,i_q + L_q \frac{di_q}{dt} + L_d p_m\, i_d\, \omega_m + K_b\, \omega_m \qquad (2)$$

where R is the motor phase resistance, p_m is the number of magnet pole pairs, ω_m is the motor shaft speed, K_b is the motor back-electromotive force coefficient, while V_d, V_q, L_d, L_q, i_d and i_q are the voltages, the inductances and the currents along the direct and the quadrant axes respectively.

The motor torque is then provided by Eq. (3),

$$T_m = [(L_d - L_q) p_m i_d + K_b] i_q \qquad (3)$$

and the system dynamics can be described with a single momentum equation, referred to the motor shaft, Eq. (4),

$$J_{tot}\,\dot{\omega}_m = T_m - T_{ext} - B_{tot}\,\omega_m - T_{f\,tot}\,\mathrm{sgn}(\omega_m) \qquad (4)$$

where

$$J_{tot} = J_m + \frac{J_g}{\tau_g^{\,2}} \qquad (5)$$

$$T_{ext} = \frac{l_s}{\tau_g} F_{ext} \qquad (6)$$

In Eq. (4), J_{tot} is the EMA inertia, B_{tot} is overall viscous damping coefficient, T_{f_tot} accounts for sliding friction effects (Coulomb, Stribeck, etc.), T_{ext} is the external loading torque, scaled to the motor shaft; while in Eqs. (5)-(6), l_s is the screw lead pitch, τ_g is the gearbox ratio, F_{ext} is the external force (coming from the dynamics and kinematics model), and J_m and J_g are the inertia of the motor shaft and gears, respectively.

Concerning the EMA control, four simply proportional loops are used (position, motor speed, direct current and quadrant current), Eqs. (7)-(10),

$$V_d = -K_i\, i_d \qquad (7)$$

$$V_q = K_i\,(i_{qi} - i_q) \qquad (8)$$

$$i_{qi} = K_\omega\,(\omega_{mi} - \omega_m) \qquad (9)$$

$$\omega_{mi} = K_x\,(x_{ai} - x_a) \qquad (10)$$

in which K_i , K_ω , K_x are the control gains of the current, speed and position loops respectively, and x_a is the actuator position, Eq. (11).

$$\dot{x}_a = \frac{l_s}{\tau_g}\omega_m \qquad (11)$$

In addition, both voltage and current demands are limited, by saturating the related values to V_{max} and i_{max} respectively.

The power balance is given by Eq. (12).

$$P_e^{(in)} = P_e^{(s)} + P_e^{(l)} + P_m^{(s)} + P_m^{(l)} + P_m^{(out)} \qquad (12)$$

In Eq. (12), $P_e^{(in)}$ is the electrical power input, $P_e^{(s)}$ is the electrical power stored in the system (only related to inductance, no capacitors are considered), $P_e^{(l)}$ is the electrical power lost in the circuitry, $P_m^{(s)}$ and $P_m^{(l)}$ are the mechanical powers stored and lost respectively, while $P_m^{(out)}$ is the mechanical power output, Eqs. (13)-(18).

$$P_e^{(in)} = V_d\, i_d + V_q\, i_q \qquad (13)$$

$$P_e^{(s)} = L_d \frac{di_d}{dt} i_d + L_q \frac{di_q}{dt} i_q \qquad (14)$$

$$P_e^{(l)} = R\,(i_d^{\,2} + i_q^{\,2}) \qquad (15)$$

$$P_m^{(s)} = J_{tot}\,\dot{\omega}_m\,\omega_m \qquad (16)$$

$$P_m^{(l)} = B_{tot}\omega_m^{\,2} + T_{f\,tot}\,\mathrm{sgn}(\omega_m)\,\omega_m \qquad (17)$$

$$P_m^{(out)} = T_{ext}\,\omega_m \qquad (18)$$

As an example, table 1 reports the basic data of the EMA system referred to the aileron control surfaces.

Parameter	Value	Unit
R	0.74	Ohm
p_m	1	-
K_b	0.4	N m / A
$L_d = L_q$	5e-3	H
$J_m = J_g$	8e-4	kg m²
l_s	8e-4	m / rad
τ_g	5.5	-
B_{tot}	4e-3	N m sec / rad
$T_{f\,tot}$	0.01	N m
K_i	9	V /A
K_ω	0.2	A sec / rad
K_x	2e5	rad / (sec m)
V_{max}	270	V
i_{max}	30	A

Tab. 1. EMA system data (aileron control surfaces)

2.4 Flight Control System dynamics and kinematics model

The same simplified architecture and the same kinematics (Figs. 3 and 4) are considered

for all the control surface (*CS*). Each *CS* is represented by a generic rigid structure rotating about an axis whose direction is assigned within the input parameters of the *CS*.

The *CS* rotation is actuated by an EMA acting on the above mentioned *CS* structure, and linked to the *CS* and to the respective wing structure by spherical hinges (points *2* and *3* Fig. 4).

The force acting on the EMA rod is calculated by taking into account the *CS* weight, the aerodynamic effects (by means of the hinge moment calculation, which refers to point *C* Fig. 4) and the effects of *CS* acceleration due to A/C manoeuvres and *CS* rotation. The *CS* mass is assumed to be concentrated in the control surface's centre of gravity (i.e.: point *H*, Fig. 4).

For each *CS*, the points *H* and *3* are assigned through their coordinates on a *CS*-fixed reference frame (*C*; X_{CS}, Y_{CS}, Z_{CS} – Fig. 3), while the origin *C* of such a frame and the point *2* are assigned through their coordinates on the A/C body-fixed reference frame (O;X_B,Y_B,Z_B, Fig. 3).

The X_{CS} axis of the *CS* reference frame coincides with the *CS* hinge axis (Fig. 3). The axis Z_{CS} is aligned with *CS* chord. The position of the origin of the *CS* reference frame (point *C* Fig. 4) is chosen in the middle point of the hinge segment.

The orientation of the *CS* reference frame is defined by the Euler's angles with respect to the body reference frame (φ_{CS}, θ_{CS}, ψ_{CS}). Such angles are defined accordingly to the classical texts of flight mechanics. Thus, the sequence of rotations which superimposes the body reference frame to the *CS* one is: ψ_{CS}, θ_{CS}, φ_{CS}.

The aerodynamic hinge moment on a generic control surface is given by:

$$H_{CS} = \frac{\rho U_{CS}^{2}}{2} mac_{f_{CS}} s_{fCS} C_{H_{CS}}(M, \mathrm{Re}_{CS}, \alpha_{CS}, \delta_{hCS}) \qquad (19)$$

where ρ is the air density, U_{CS} is the local airspeed magnitude, mac_{fcs} is the mean aerodynamic chord of the *CS* considered as an isolated wing, s_{fcs} is the span of the flapped portion of the aerodynamic surface under consideration (wing, horizontal tail or rudder) and C_{Hcs} is the hinge moment coefficient. The last coefficient is assumed to be a function of the Mach number (*M*), the Reynolds number (Re_{CS}), evaluated by means of the mean aerodynamic chord of the aerodynamic surface containing the specific *CS* and the local airspeed, the local angle of attack (α_{CS}) and the deflection of the control surface (δ_{hcs}).

The hinge moment coefficient (C_{Hcs}) depends both on incidence (α_{CS}) and on control deflection (δ_{hcs}) through relations that are generally nonlinear. Typically, the flight control dynamics is studied with reference to small control deflection (<10°), where a linear relation can be used. This approach is not adequate for the purpose of this study, where extreme operations have to be examined. The envelopes of deflection of the aircraft control surfaces exceed the linear limits, thus the hinge moment model is based on the following assumptions:

a) the linear range with respect to the control deflection is: $|\delta_{h\,CS}| \le \delta^{lin}$
b) out of the linear range, the hinge moment coefficient derivative b_{2hcs} grows linearly with δ_{hcs}, and doubles its value for a control deflection equal to δ^{double}
c) the contribution of δ_{hcs} to the hinge moment coefficient, for high control deflections, is limited by a "saturation function", that is $C_{H_{CS}}|^{sat} \le K_{CS}^{sat} \cdot \sin(\delta_{hCS})$

By applying these assumptions, the evaluation of hinge moments for the control surfaces is provided by the following relation:

$$\begin{aligned} C_{H_{CS}} &= C_{H0_{CS}} + b_{1CS}(M, \mathrm{Re}_{CS}) \cdot \alpha_{CS} \\ \vdots \quad &\quad + b_{2hCS}(M, \mathrm{Re}_{CS}, \delta_{hCS}) \cdot \delta_{hCS} \end{aligned} \qquad (20)$$

where b_{1cs} is a constant coefficients evaluated as a function of *M* and Re_{CS}, while b_{2hcs} is evaluated

$$\begin{cases} b_{2CS}(M, Re_{CS}) & for\,|\delta_{hCS}| \le \delta^{lin} \\ b_{2CS}(M, Re_{CS}) \cdot \left[1 + \dfrac{|\delta_{hCS}| - \delta^{lin}}{\delta^{double} - \delta^{lin}}\right] & for\,|\delta_{hCS}| \ge \delta^{lin} \end{cases} \qquad (21)$$

In addition the product $b_{2hCS}(M, \mathrm{Re}_{CS}) \cdot \delta_{hCS}$ is limited by the following saturation function:

$$|b_{2hCS}(M, \mathrm{Re}_{CS}) \cdot \delta_{hCS}| \le |K_{CS}^{sat} \cdot \sin(\delta_{hCS})| \qquad (22)$$

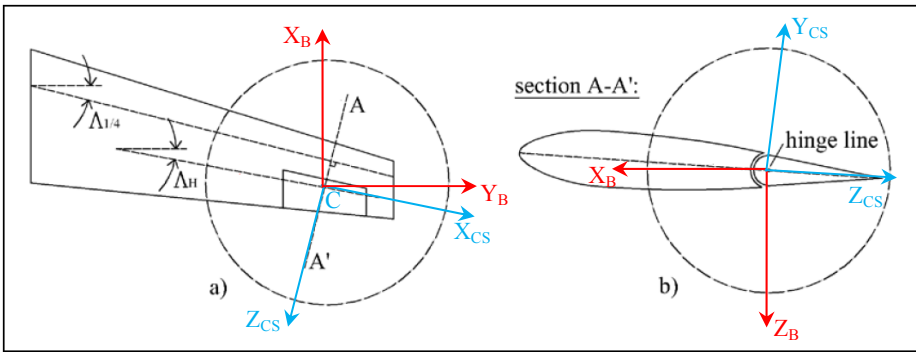

Fig. 3. Control surface general architecture

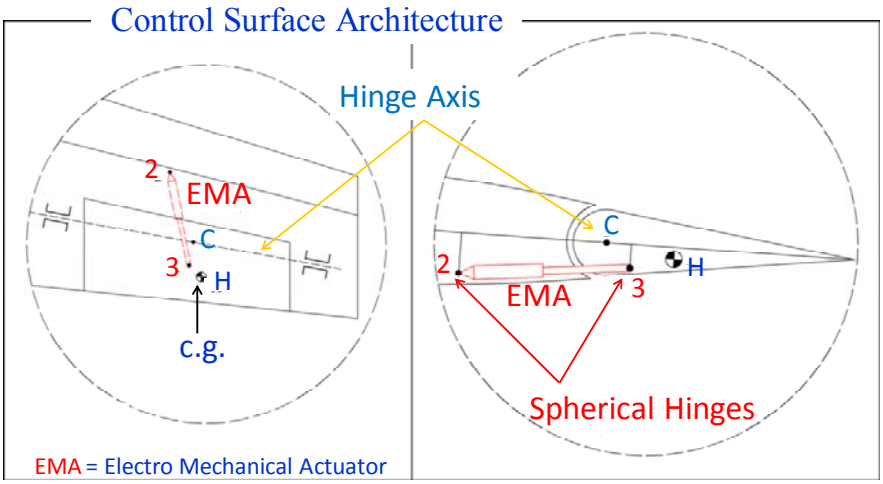

Fig. 4. Reference frames and characteristic points of the generic *CS* (ref. to Fig. 3)

The coefficients depending on the Mach number and the Reynolds number have been calculated by means of the ESDU method [8][9] on the basis of the Net equivalent wing geometry. Figure 5 shows a diagram of the variation of the hinge moment coefficient (C_{Hcs}) with respect to control deflection (δ_{hcs}) for a given Mach number and a given incidence of the control surface (α_{cs}).

3 Simulation tests

A simulation test is presented in this section, as examples of assessment of FCS power flows in severe operative conditions. In this test, the commands are provided in levelled flight conditions, at A/C speed of 100 m/sec, A/C load factor of 2.5 and with zero angle-of-attack and sideslip. The command deflections are characterized by large amplitudes and speeds (Fig. 6) and, for each *CS*, a motion inversion is

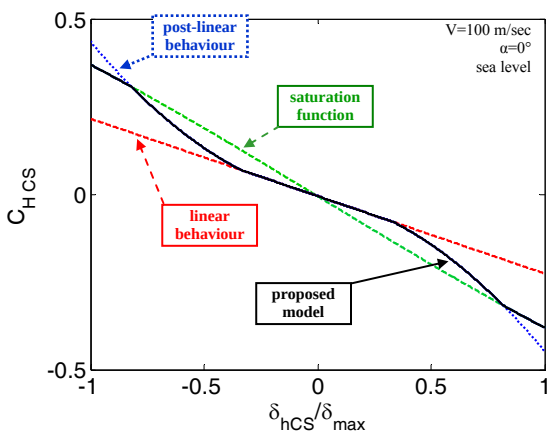

Fig. 5 - Hinge moment coefficient with respect to control deflection (aileron example)

imposed when the actuators achieves the maximum deflections (maximum hinge moments). In addition, such commands have been built in order to synchronize the control surfaces power peaks, thus to have an

assessment of the maximum FCS power requests.
Even if it could be argued that this test is referred to excessively severe conditions (e.g. contemporary extreme deflections on all *CS*s), this approach provides an estimation of the maximum system power flows, by using the systems specifications only.

4 Results

Figure 7 shows the power flows for each *CS* of the FCS. The models evaluate identical power flows for EMAs driving the *CS*s located symmetrically with respect to the A/C longitudinal plane (e.g. left and right ailerons), for the same commanded deflections. For this reason, all the power flows of Fig. 7, except those referred to rudder (single surface) are the sum of equal contributes. In addition, it is relevant to observe that the aerodynamic interaction among the different *CS* is neglected, while the flaps deflection modifies the total lift coefficient that affects the down-wash angle and the Elevators aerodynamic.

Figure 7 highlights the phases in which the EMAs work in brake mode (negative mechanical power) or in motor mode (positive mechanical power). In the test, the total maximum FCS power absorption ranges about 20 kW, and this value can be considered as a reference also for the maximum generated power.

Figure 8 reports the Fast Fourier Transform (FFT) of the total FCS power absorption signal coming from the considered test. The plot points out that the frequency content of the power absorption signal, apart from the low frequency range (<1 Hz) where it is essentially dominated by the FCS demand signals, is relevant (components greater than 100 W) up to 30 Hz.

5 Conclusions

The developed models, referred to an aircraft with a flight control system with thirteen control surfaces, are used within the Clean Sky GRA project as sub-models of a Shared Simulation Environment, which is a tool able to support the design and the validation of the electrical energy management strategies.

The dynamics and kinematics models of each flight control surface take into account inertial (A/C manoeuvres and load motions), weight and aerodynamic hinge moment contributions.

The test is referred to severe operating conditions (high load factor, flight controls commanded with large-amplitude/high-speed demands and motion inversion at maximum deflections), to identify the maximum electric power flows. In terms of total power absorption, the FCS requires about 20 kW peak power, and the frequency content of the power signal can be considered relevant (FFT components greater than 100 W) up to 30 Hz. It is worth noting that these power signal characteristics are roughly valid for both motor and brake operation of the actuators, so this power amounts must be handled by dissipation systems (or regeneration systems, if present).
The analysis highlighted that the electric power flows of flaps are essentially dominated by the mechanical power output, since the EMA motions are characterised by low speed/high torque cycles. On the other hand, the electric power flows of primary flight controls (ailerons, elevators, rudder, spoilers) also depend on transient mechanical power, producing peaks when high speed motions are required to the EMAs.

Acknowledgements

This work was partially granted under the Green Regional Aircraft ITD, All Electric Aircraft domain, of the Clean Sky JTI, within the European framework Program 7. The authors gratefully acknowledge the support by Clean Sky, the European Commission and all the partners involved into the All Electric Aircraft domain.

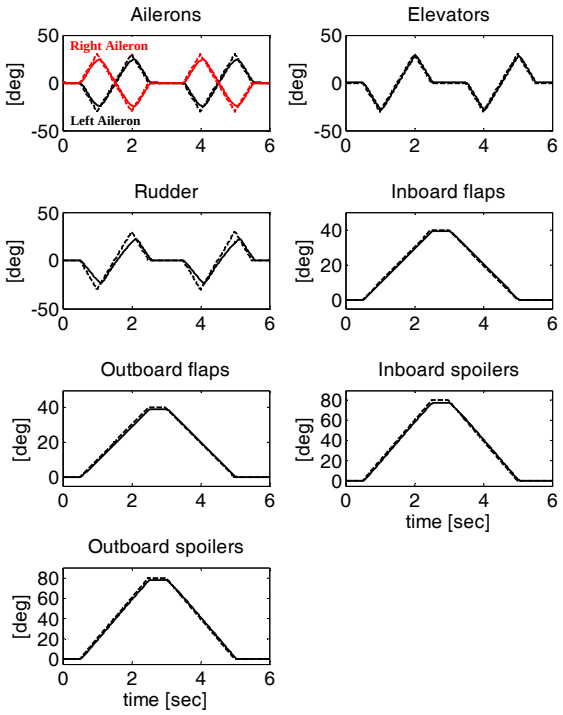

Fig. 6 FCS position dynamics

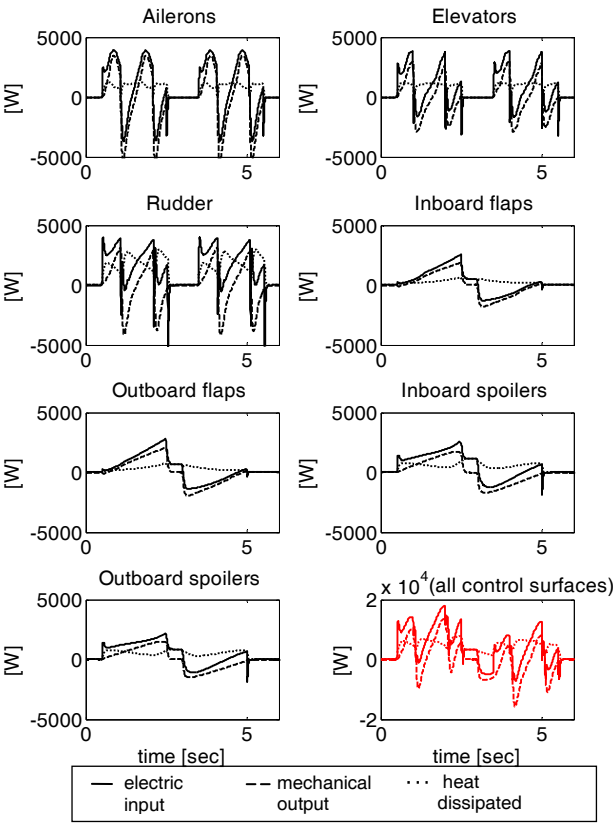

Fig. 7 FCS power flows

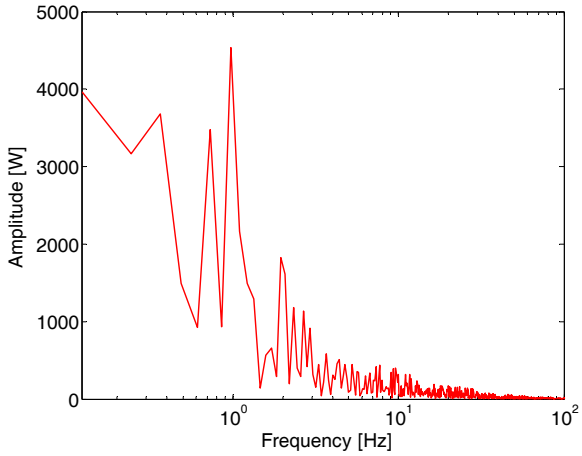

Fig. 8 FFT of the total FCS power absorption signal

References

[1] Emadi A. and Ehsani M.. "Aircraft power systems: technology, state of the art, and future trends", IEEE AES Systems Magazine, January 2000, pp. 28-32.

[2] Cutts S. J.. "A collaborative approach to the more electric aircraft", IEE Conference on Power Electronics, Machines and Drives, Bath (UK), 2002, pp. 223-228.

[3] Howse M.. "All electric aircraft", IEE Power Engineering Journal, Vol. 17, No. 4, 2003, pp. 35–37,.

[4] Rosero J. A., Ortega J. A., Aldabas E. and Romeral L. "Moving towards a more electric aircraft", IEEE A&E Systems Magazine, March 2007, pp. 3-9.

[5] Maldonado M. A. and Korba G. J.. "Power management and distribution system for a more electric aircraft (MADMEL) - Program status", IEEE AES Systems Magazine, December 1999, pp. 3-8.

[6] Schallert C., Pfeiffer A. and Bals J.. "Generator power optimisation for a more electric aircraft by use of a virtual iron bird", 25th International Congress of Aeronautical Sciences (ICAS), Hamburg (Germany), 2006.

[7] Anastasio V. and Di Donna L.. "Power by wire meets environmental friendly requirements", XIX AIDAA National Congress, Forlì (Italy), 2007.

[8] Hinge moment coefficient derivatives for trailing-edge controls on wings at subsonic speeds – Educational Science Data Unit 89009.

[9] Example of procedure in calculation of control hinge moments – Educational Science Data Unit 89010.

Contact Author Email Address

f.schettini@ing.unipi.it

Copyright Statement

The authors confirm that they, and/or their company or organization, hold copyright on all of the original material included in this paper. The authors also confirm that they have obtained permission, from the copyright holder of any third party material included in this paper, to publish it as part of their paper. The authors confirm that they give permission, or have obtained permission from the copyright holder of this paper, for the publication and distribution of this paper as part of the ICAS 2014 proceedings or as individual off-prints from the proceedings.